



ELSEVIER

15 March 2002

Optics Communications 203 (2002) 197–211

OPTICS
COMMUNICATIONS

www.elsevier.com/locate/optcom

Optical reticle trackers with the multi-source discrimination capability by using independent component analysis

Ivica Kopriva^{a,*}, Harold Szu^a, Antun Peršin^b

^a *Department of Electrical and Computer Engineering, Digital Media RF Laboratory – Room 308, George Washington University, 725 23rd Street NW, Washington, DC 20052, USA*

^b *Rudjer Boskovic Institute, P.O. Box 180, 10002 Zagreb, Croatia*

Received 24 November 2001; received in revised form 8 January 2002; accepted 9 January 2002

Abstract

Due to the simplicity and low cost, since only a few detectors are used, reticle trackers are still in use and are subject of further research. However, the major disadvantage of the reticle trackers has been proven to be sensitivity on the man-made clutters such as flares or jammers. To resolve this problem a beam splitter based modification of the optical trackers has been used successfully for tracking and discrimination of the several moving incoherent (heat) optical sources in the mathematical framework called independent component analyses (ICA). Here we further explore the theoretical basis of the coherent and partially coherent illumination by laser for the possibility of blind source demixing. An application of the partial coherence theory and Huygens–Fresnel principle is utilized to formulate the problem. When incoherence is assumed a linear ICA model is obtained while in the most general case of either partially or totally coherent optical radiation the resulting signal model is inherently nonlinear. It can be transformed into linear one under very special condition that assumes no relative motion between the radiating sources. In the most general case of partially coherent radiation, tracking of the several moving optical sources by using the beam splitter based reticle trackers is possible either by using ICA algorithms developed for undercomplete representation or by introduction of one additional sensor. The three conditions necessary for the ICA theory to work (statistical independence and non-Gaussianity of the source signals and nonsingularity of the mixing matrix) are shown to be fulfilled in principle for any kind of the reticle geometry. In relation to some IR counter-countermeasures algorithms which are based on the heuristic and sometimes unrealistic assumptions (target performs no maneuvering) the approach exposed here has been proven to be theoretically consistent without any special constraints imposed on the optical sources. © 2002 Elsevier Science B.V. All rights reserved.

PACS: 07.05.D; 07.05.M; 85.60; 42.50.M

Keywords: Independent component analysis; Unsupervised neural networks; Blind system identification; Infrared reticle trackers

* Corresponding author. Tel.: +202-994-0880; fax: +202-994-5171.
E-mail address: ikopriva@seas.gwu.edu (I. Kopriva).

1. Introduction

Reticle trackers are considered to be the classical approach for estimating the position of a target in a considered field of view (FOV) and are widely used in IR seekers [3–14]. Their advantage is simplicity and low cost [10,11]. However, the major drawback of the reticle trackers has been proven to be sensitivity on the man-made clutters such as flares and jammers [8,10]. Such limitation of the reticle systems in the real world applications was very often due to the use of the single detector element [10]. Several attempts to neutralize such a problem are based on the introduction of the segmented focal plane arrays (FPA) behind the reticle [10,14].

Since the advantage of the reticle seekers is simplicity and low cost the segmented FPA must be comprised of a small number of detectors so as not to become as complex and expensive as an imaging system with a full strength FPA. The problem still exists when the two sources are in the space region acquired by the same detector element. An appropriate space resolution should be ensured by using more detector elements. A new approach proposed in [3,7] was extended in [4–6] and will be completed in this paper. It is based on the independent component analysis (ICA) theory and an appropriate modification of the optical tracker design. We present in Section 2 a brief description of the optical modulation theory while more details can be found in [8–13]. In Section 3 a rigorous derivation of the signal model of the modified optical tracker output signals is given. Motivated by the advent of the Laser Radar, LI-DAR, we explore the general case of the blind discrimination capability of the moving coherent and partially coherent laser sources or the incoherent heat sources. An application of the statistical optics principles, the partial coherence theory and the Huygens–Fresnel principle [1,2], is utilized to formulate the problem. Although, the linear ICA is obtained as a special solution for the incoherent sources this case is of practical interest. Therefore, we address in Section 4 the problem of the characterization of the linear part of the signal model derived in Section 3. By using blind identification approach [21], we show that the convolutive mixing model could be non-minimum phased.

We propose an adaptive frequency domain algorithm for separating experimental data obtained from the modified optical tracking device [24]. In Section 5 the experimental results are presented for the incoherent heat sources while conclusions are given in Section 6.

2. Optical modulation theory

The reticle system provides directional information for tracking and also suppresses unwanted background signals [8,9], by performing modulation of the incident light flux. According to the type of the reticle and the relative motion produced by the scan pattern, the encoding method of the reticle may be classified into AM, FM and pulse code modulation. In addition, according to how the relative motion between the reticle and the optical spot is obtained we may classify reticle systems into fixed or moving reticle. When reticle is fixed the relative motion can be obtained by using rotating mirror which causes the light beam and hence the spot to either nutate or rotate in relation to the fixed reticle. In the opposite case spot forming optics is fixed while reticle performs either nutation [3,8,9] or spinning, [12,13]. The general case of the moving reticle system is illustrated with Fig. 1. The moving reticle is placed in the focal plane of the collecting optics, while field optics collects modulated light and focuses it on the detector. The selective amplifier center frequency is usually the number of spoke pairs times the nutation or spinning frequency. The rising-sun reticle that is very often used in the nutating FM reticle trackers [3,8,9] is shown in Fig. 2. In a case of either nutation or spinning the detector output voltage is proportional to the light irradiance behind the reticle according to [12,13]

$$I(t) = I_p \int_0^R \int_{-\pi}^{\pi} s(r, \varphi) \delta[r - r_0, \theta - (\Omega t - \varphi_0)] r \, d\varphi \, dr, \quad (1)$$

where $s(r, \varphi)$ is the reticle transmission function (rtf) and r and φ are spatial variables of the rtf ranging from 0 to R and $-\pi$ to π , respectively. Also let the reticle nutation or spinning rate be Ω

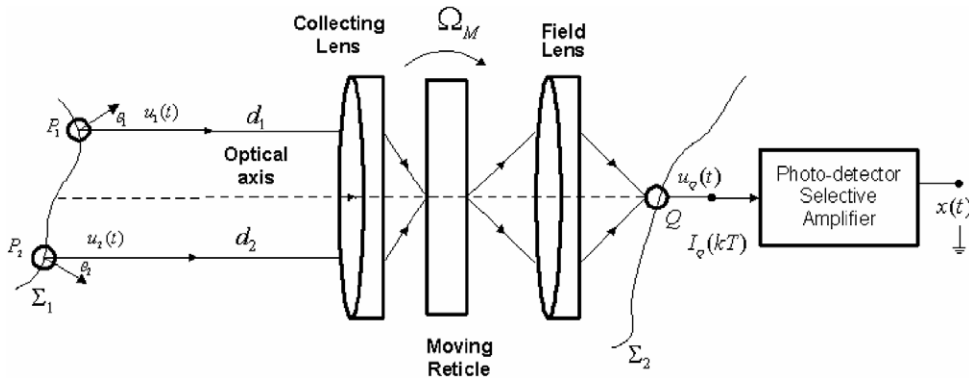


Fig. 1. The moving reticle based optical tracker.

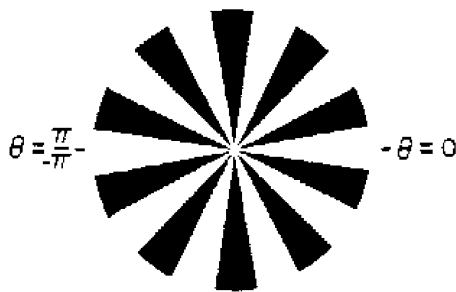


Fig. 2. The rising-sun reticle.

in rads^{-1} and let r_0 and θ_0 be the spatial coordinates of a point source that is imaged onto the reticle. I_P in (1) is the peak irradiance of the point source through the rtf. Since the convolution of any function with delta function is the function located at the delta function coordinates Eq. (1) becomes

$$I(t) = I_P s(r_0, \Omega t - \varphi_0). \tag{2}$$

We shall derive Eq. (2) in Section 3 as a limiting case of the multi-source scenario by using more general approach based on the statistical optics principles, the partial coherence theory and the Huygens–Fresnel principle of the propagation of electromagnetic waves [1,2]. In a case of the optical trackers that generate FM signal by means of the rising-sun reticle, Fig. 2, and nutation the rtf are of the form [9,11]

$$s(r, \varphi, t) = I_P \cos[m\Omega t - m(r/a) \sin(\varphi)]. \tag{3}$$

The optical spot performs circular motion, with radius a , around the center with coordinates (r, φ) relative to the center of the reticle. Necessary condition for Eq. (3) to hold is $(r/a)^2 \ll 1$. m in Eq. (3) is the number of spoke pairs of the reticle. Eq. (3) represents canonical form of the FM signal where frequency deviation from the carrier frequency is directly proportional with the spot r coordinate. So by using nutating rising-sun reticle, both directional information distance and azimuth are encoded in the reticle transmission function. Instead of using nutation the relative motion between the spot and the reticle can be obtained by simple rotation or spinning.

That happens when according to Eq. (3) $r = 0$ while a represents spot radial coordinate. It is obvious from Eq. (3) that reticle transmission function is reduced on the pure cosine being invariant of the spot coordinates. It means that the rising-sun reticle cannot be used for encoding the optical spot position in the spinning case, nevertheless, whether FM or AM modulation is used. A lot of other spoke geometries is proposed for that purpose [12,13]. It has been shown in [12] that rtf of the spinning FM reticle can be written in general form as

$$s(r, \theta) = \frac{1}{2} + \frac{1}{2} \cos \left[m(r) \int_0^{\theta + \rho(r)} f(\alpha) d\alpha \right]. \tag{4}$$

The $1/2$ dc term in Eq. (4) allows an average reticle transmission of $1/2$ rather than zero (i.e. no light passing the reticle). The spinning FM reticles can be completely described by these three parameters:

frequency vs. angle $f(\theta)$, frequency vs. radius $m(r)$ and phase or spoke function $\rho(r)$. To use a spinning reticle for finding a target in both the radial and azimuth direction at least nonconstant $f(\theta)$ and $m(r)$ parameters must be imposed on the reticle. Such reticle is shown in Fig. 3. The spatial transmission function of this reticle is

$$s(r, \theta) = \frac{1}{2} + \frac{1}{2} \cos \left\{ m \frac{r}{R} [\theta + 0.4 \sin(\theta)] \right\}. \quad (5)$$

Because an FM signal is known to be superior to an AM signal with regard to signal quality, that is it suffers less noise interference, the FM reticles are generally of greater interest. Nevertheless, the AM reticles are used in IR missile seekers especially in the surface-to-air and air-to-air environments. It has been shown in [13] that it is possible to describe spinning AM reticles using three amplitude parameters (similarly to the previously described FM parameters): amplitude vs. angle $f(\theta)$, amplitude vs. radius $g(r)$, and phase $\rho(r)$. The general AM equation is given by [13]

$$S(\theta) = \frac{1}{2} + V[1 + mf(\theta)] \cos(k\theta), \quad (6)$$

where $S(\theta)$ is the modulated signal, V is the constant, m is the modulation index, $f(\theta)$ is the low frequency modulation signal and k is the carrier frequency that corresponds with the number of spoke pairs. Like in the FM reticle case the $1/2$ dc term in Eq. (6) allows an average reticle transmission of $1/2$ rather than zero (i.e., no light passing the reticle). Reticle that encodes both the target radial and angular position shown in Fig. 4 with a spatial transmission function is given by

$$s(r, \theta) = \frac{1}{2} + \frac{1}{4} \frac{r}{R} (1 + \cos \theta) \cos(30\theta). \quad (7)$$

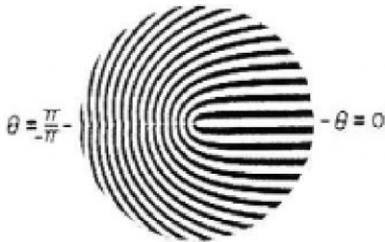


Fig. 3. Frequency vs. radius and angle [12].

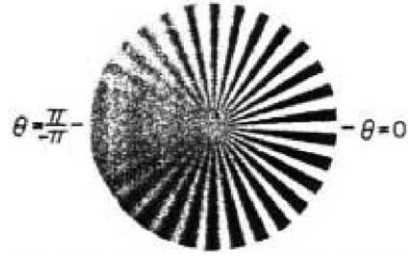


Fig. 4. Amplitude vs. radius and angle [13].

More details about the reticle tracking systems can be found in [8–14].

3. Derivation of the signal model

We shall assume the scenario shown in Fig. 1. Intensity at point Q (detector) is obtained as

$$I_Q = \langle u(Q, t) u^*(Q, t) \rangle, \quad (8)$$

where

$$u(Q, t) = u(Q_1, t) + u(Q_2, t) \quad (9)$$

and $u(Q_1, t)$ is disturbance at the point Q due to the point P_1 in the plane Σ_1 and $u(Q_2, t)$ is disturbance at the point Q due the point P_2 in plane Σ_1 . Those quantities can be obtained as functions of the radiation at the points P_1 and P_2 by application of the Huygens–Fresnel principle to the propagation of the optical waves. Relation will be derived for the quantity $u(Q_1, t)$ while for $u(Q_2, t)$ the full analogy applies. We shall give derivation for the quasi-monochromatic or narrow-band light since it is of the practical interest. The purely monochromatic case is obtained as a special case of the quasi-monochromatic derivation. If the light is quasi-monochromatic, then [1,2]

$$u(Q_1, t) = \int \int_{\Sigma_1} \frac{u(P_1, t - d_1/c)}{d_1} K(P_1, Q_1) A_1 dP_1, \quad (10)$$

where A_1 is the inclination factor that for the small diffraction angle θ_1 can be approximated with $A_1 = 1/j\tilde{\lambda}$, where $\tilde{\lambda}$ is central wavelength of the source emitting band. Because the optical system is present between Σ_1 and Σ_2 its influence is taken

into account introducing $K(P_1, Q_1)$ into the integral (10). We shall assume here the ideal lenses and only rtf to be important so that

$$K(P_1, Q_1) \cong s(r_1, \Omega t - \varphi_1). \tag{11}$$

Now intensity I_Q in Eq. (8) is obtained as

$$\begin{aligned} I_Q &= \langle u(Q_1, t)u^*(Q_1, t) \rangle + \langle u(Q_2, t)u^*(Q_2, t) \rangle \\ &+ \langle u(Q_1, t)u^*(Q_2, t) \rangle \\ &+ \langle u^*(Q_1, t), u(Q_2, t) \rangle. \end{aligned} \tag{12}$$

The first two parts in Eq. (12) represent intensities produced by the optical sources placed at the points P_1 and P_2 , respectively. Then for the quasi-monochromatic light it applies

$$\begin{aligned} I(Q_1, t) &= \langle u(Q_1, t)u^*(Q_1, t) \rangle \\ &= \frac{1}{\lambda^2} \int \int_{\Sigma_1} \int \int_{\Sigma_1} \frac{I(P_1, t)}{d_1^2} dP_1 dP_1 \\ &\times s(r_1, \varphi_1, t). \end{aligned} \tag{13}$$

If we assume a point source at P_1 , then

$$u\left(P_1, t - \frac{d_1}{c}\right) = u\left(P_1, t - \frac{d_1}{c}\right) \delta(|P - P_1|). \tag{14}$$

Then Eq. (13) is reduced to

$$I(Q_1, t) = \frac{1}{\lambda^2} \frac{I(P_1, t)}{d_1^2} s(r_1, \varphi_1, t). \tag{15}$$

In Eqs. (13) and (15) as well as in analogous subsequent derivations it will be assumed that [4,5]:

$$\begin{aligned} s^2(r_1, \varphi_1, t) &= s(r_1, \varphi_1, t), \\ \langle s(r_1, \varphi_1, t) \rangle &= s(r_1, \varphi_1, t). \end{aligned}$$

Derivation of the third and fourth part in Eq. (12) is becoming especially interesting. For a narrow-band light it applies the following

$$\begin{aligned} \langle u(Q_1, t)u^*(Q_2, t) \rangle &= \frac{1}{\lambda^2 d_1 d_2} \int \int_{\Sigma_1} \int \int_{\Sigma_1} \Gamma\left(P_1, P_2, t - \frac{d_2 - d_1}{c}\right) \\ &\times dP_1 dP_2 \times s(r_1, \varphi_1, t)s(r_2, \varphi_2, t). \end{aligned} \tag{16}$$

For the $\langle u^*(Q_1, t)u(Q_2, t) \rangle$ the same expression is obtained so it will not be derived. According to [2, pp. 180 and 197, Eqs. (5.2-31) and (5.4-7)] it applies for the quasi-monochromatic light

$$\Gamma\left(P_1, P_2, \frac{d_2 - d_1}{c}\right) = J(P_1, P_2) \exp\left[-j\frac{2\pi}{\lambda}(d_2 - d_1)\right]$$

and Eq. (16) becomes

$$\begin{aligned} \langle u(Q_1, t)u^*(Q_2, t) \rangle &= \frac{1}{\lambda^2 d_1 d_2} \int \int_{\Sigma_1} \int \int_{\Sigma_1} J(P_1, P_2) \\ &\times \exp\left[-j\frac{2\pi}{\lambda}(d_2 - d_1)\right] \\ &\times dP_1 dP_2 \times s(r_1, \varphi_1, t)s(r_2, \varphi_2, t), \end{aligned} \tag{17}$$

where $\Gamma(P_1, P_2, \tau)$ is the mutual coherence and $J(P_1, P_2)$ is the mutual intensity of light at the points P_1 and P_2 . According to [2, p. 181, Eqs. (5.2-30)–(5.2-33)] and [1, p. 507, Eqs. (9) and (10)] the mutual intensity can be expressed as

$$\begin{aligned} J(P_1, P_2) \exp\left[-j\frac{2\pi}{\lambda}(d_2 - d_1)\right] &= \sqrt{I(P_1)I(P_2)}\gamma_{12}(0), \end{aligned}$$

where $\gamma_{12}(0)$ is the mutual degree of coherence of the two sources u_1 and u_2 in the plane Σ_1 . Then Eq. (17) is transformed into

$$\begin{aligned} \langle u(Q_1, t)u^*(Q_2, t) \rangle &= \frac{1}{\lambda^2 d_1 d_2} \int \int_{\Sigma_1} \int \int_{\Sigma_1} \sqrt{I(P_1, P_2)}\gamma_{12}(0) dP_1 dP_2 \\ &\times s(r_1, \varphi_1, t)s(r_2, \varphi_2, t). \end{aligned} \tag{18}$$

Assuming point sources at the points P_1 and P_2 we finally obtain

$$\begin{aligned} \langle u(Q_1, t)u^*(Q_2, t) \rangle &= \frac{1}{\lambda^2 d_1 d_2} \sqrt{I(P_1, P_2)}\gamma_{12}(0) \\ &\times s(r_1, \varphi_1, t)s(r_2, \varphi_2, t). \end{aligned} \tag{19}$$

From [1, pp. 507–508, Eqs. (9)–(13)] and [2, pp. 181 and 205, Eqs. (5.2-37) and (5.5-14)–(5.5-16)] it applies for the quasi-monochromatic source

$$\gamma_{12}(0) = |\gamma_{12}(0)| \cos(\beta_{12}), \tag{20}$$

where

$$\beta_{12} = \arg \gamma_{12}(0) = \Phi(P_2) - \Phi(P_1) \tag{21}$$

and for the moving quasi-monochromatic sources it can be written

$$\gamma_{12}(t) = |\gamma_{12}(t)| \cos\left[2\pi\frac{v}{\lambda}t + \Delta\Phi\right], \tag{22}$$

where v is relative velocity between the two points and $\Delta\Phi$ is some initial phase difference. Now Eq. (18) can be written as

$$\begin{aligned} & \langle u(Q_1, t)u^*(Q_2, t) \rangle \\ &= \frac{1}{\bar{\lambda}^2 d_1 d_2} \sqrt{I(P_1, P_2)} \times \gamma_{12}(t) s(r_1, \varphi_1, t) s(r_2, \varphi_2, t), \end{aligned} \tag{23}$$

where $\gamma_{12}(t)$ is given with Eq. (22) for the quasi-monochromatic radiation and is in principle the unknown function of time for the polychromatic radiation. Eq. (23) can be applied on the pure monochromatic sources replacing $\bar{\lambda}$ with λ_0 . The photo-current is obtained when the intensity I_Q , Eq. (12) and the related Eqs. (15) and (23), is expressed in terms of the spectral irradiance and when detector spectral responsivity is taken into consideration giving for the quasi-monochromatic and purely monochromatic sources

$$\begin{aligned} i(t) &= \frac{A}{\bar{\lambda}^2} \frac{I(P_1, \bar{\lambda}, t)}{d_1^2} R(\bar{\lambda}) \times s(r_1, \varphi_1, t) \\ &+ \frac{A}{\bar{\lambda}^2} \frac{I(P_2, \bar{\lambda}, t)}{d_2^2} R(\bar{\lambda}) \times s(r_2, \varphi_2, t) \\ &+ \frac{1}{\bar{\lambda}^2 d_1 d_2} \sqrt{I(P_1, \bar{\lambda}, t) I(P_2, \bar{\lambda}, t) \gamma_{12}(t)} \\ &\times s(r_1, \varphi_1, t) s(r_2, \varphi_2, t), \end{aligned} \tag{24}$$

where A is the detector sensing area and $R(\bar{\lambda})$ is the detector, responsivity. Eq. (24) will be the basis for

obtaining expressions for the optical tracker output signals.

Let the modified tracker be illustrated with Fig. 5 [3–7]. The reason for using more detectors is the inability of the existing tracker, Fig. 1, to discriminate more optical sources [3–14]. On the basis of Eq. (24) the photo-currents i_1 and i_2 can be obtained by simply inserting $\tau(\lambda)$ and $\rho(\lambda)$ in (24), where $\tau(\lambda)$ is the beam splitter transmission coefficient and $\rho(\lambda)$ is the beam splitter reflection coefficient. The optical tracker output signals x_1 and x_2 are obtained as

$$x_j(t) = g_j(t) * i_j(t), \quad j \in \{1, 2\}, \tag{25}$$

where g_1 and g_2 are impulse responses of the selective amplifiers and $*$ means temporal convolution. Based on Eq. (24) the following is obtained for the quasi-monochromatic and monochromatic sources

$$\begin{aligned} x_1(t) &= g_{11}(t) * s(r_1, \varphi_1, t) + g_{12}(t) \\ &* s(r_2, \varphi_2, t) + g_{13}(t) \\ &* [\gamma_{12}(t) \times s(r_1, \varphi_1, t) s(r_2, \varphi_2, t)] \\ x_2(t) &= g_{21}(t) * s(r_1, \varphi_1, t) + g_{22}(t) \\ &* s(r_2, \varphi_2, t) + g_{23}(t) \\ &* [\gamma_{12}(t) \times s(r_1, \varphi_1, t) s(r_2, \varphi_2, t)], \end{aligned} \tag{26}$$

where expressions for the impulse responses $g_{ij}(t), j \in \{1, 2, 3\}$ are given in [4,5]. Due to the high level of non-stationarity we were not able to

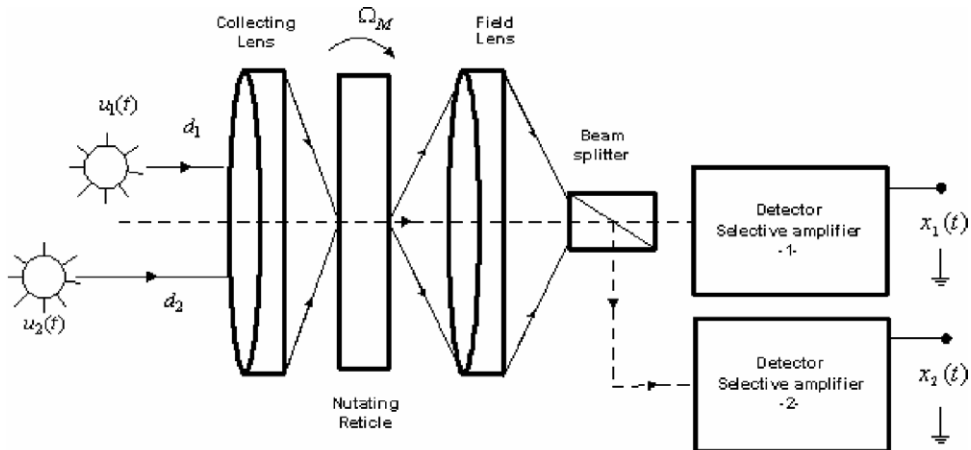


Fig. 5. The modified optical tracker.

include in Eq. (26) the mutual degree of coherence $\gamma_{12}(t)$ as the part of the impulse responses. The general approach to work with nonlinear mixtures is to apply ICA algorithms developed for the nonlinear models such as [18–20]. However, we shall exploit here the special properties of the physical model of the optical tracking system that makes it possible to use linear ICA algorithms. The signal model equation (26) is reduced into the linear one when the optical sources are incoherent i.e. $\gamma_{12}(t) = 0$ [3–7]. Also, if $\gamma_{12}(t) = \text{const.}$ the signal model equation (26) is transformed into the linear one by simple linear bandpass filtering [4,5]. In the most general case when $\gamma_{12}(t)$ is some arbitrary function of time we can introduce additional artificial source signal: $s_3(t) = \text{Re}[\gamma_{12}(t)] \times s_1(t) s_2(t)$. We can either use the ICA method developed for undercomplete representation (i.e. more sources than sensors) [27], in order to recover the three source signals from the two measured signals or to introduce one additional beam splitter and one additional detector in order to recover the three unknown source signals on the basis of three measured signals. We can discard the source signal s_3 after recovery since we are not interested in it. Since the first two source signals are sub-Gaussian signals the third source signal can be even Gaussian. That fulfills the non-Gaussianity requirement for the ICA theory to work. The second requirement is the statistical independence between the source signals. It has been shown in [3] that this requirement is fulfilled for the source signals s_1 and s_2 . The third requirement is the non-singularity of the mixing system equation (26) and it has been shown in [3] that this requirement is also fulfilled if the beam splitter transmission coefficient satisfies $\tau(\lambda) \neq \text{const.}$ in the wavelength region of interest what turns out to be always satisfied. We have to show now that the artificial source signal s_3 is statistically independent in relation to the first two source signals. For the two FM signals generated by the nutating rising-sun reticle system, Fig. 2, Fig. 6 shows the autocorrelation function $c_2(s_1)$ while the cross-correlation function $c_{11}(s_1, s_3)$ is shown in Fig. 7. The fourth-order cumulant $c_4(s_1)$ is shown in Fig. 8 while the fourth-order cross-cumulant $c_{22}(s_1, s_3)$ is shown in Fig. 9. It can be noticed that the second- and fourth-order cross-

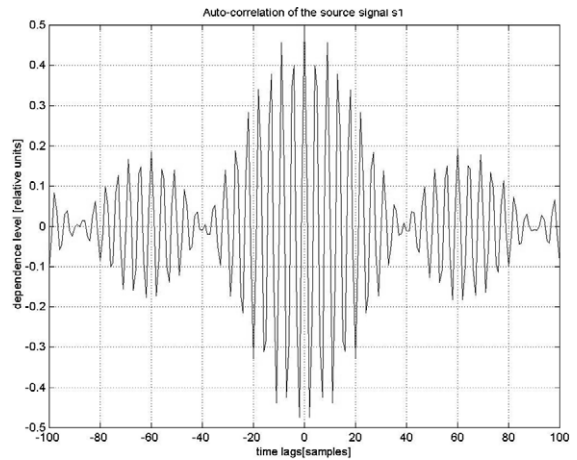


Fig. 6. The autocorrelation function $c_2(s_1)$.

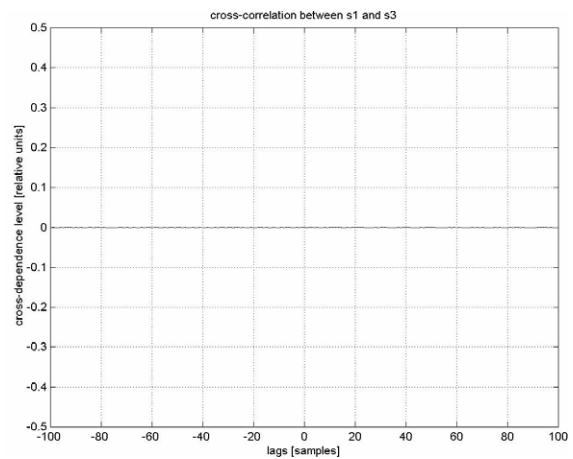


Fig. 7. The cross-correlation function $c_{11}(s_1, s_3)$.

cumulants between s_1, s_2 and s_3 are more than 10 times smaller than the related second- and fourth-order cumulants. One can also note that in the special case of the quasi-monochromatic radiation, Eq. (22), for $\bar{\lambda} = 1 \mu\text{m}$ and relative velocity $v > 0.1 \text{ ms}^{-1}$ the numerical frequency $f = v/\bar{\lambda}$ is greater than 100 kHz in which case the nonlinear part in Eq. (26) is transformed on the higher frequencies that are out of the pass-band region of the bandpass filters g_{13} and g_{23} so that the signal model equation (26) could be again reduced on the linear one by using linear bandpass filters.

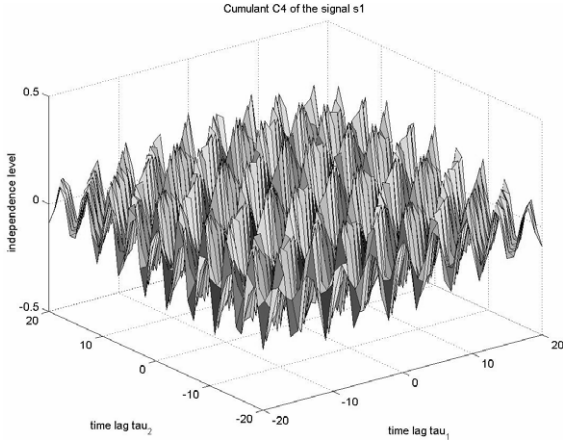


Fig. 8. The fourth-order cumulant $c_4(s_1)$.

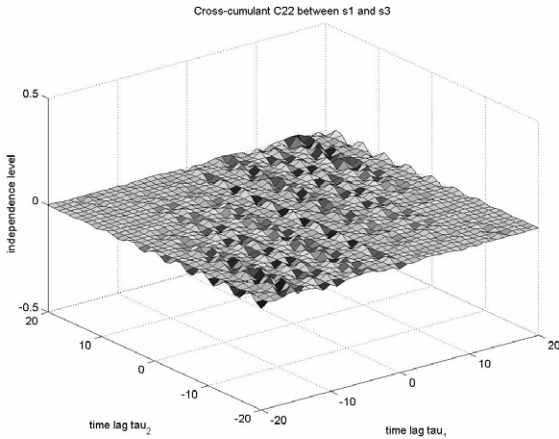


Fig. 9. The fourth-order cross-cumulant $c_{22}(s_1, s_3)$.

4. Characterization of the signal model and blind source separation algorithm

Since we have shown that the nonlinear model (26) can in principle be reduced onto the linear one we shall assume the linear form of the signal model (26) i.e. that optical sources are mutually incoherent with $\gamma_{12}(t) = 0$. There are two problems associated with the statistical inversion of the convolutive mixtures, Fig. 10 and Eq. (26): the whitening problems and problems with the non-minimum phase of the mixing system transfer function. The whitening problem can be solved by

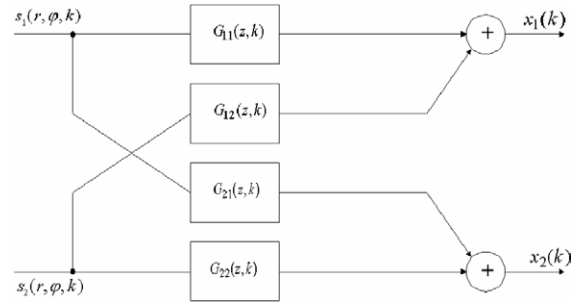


Fig. 10. Convolutive signal model.

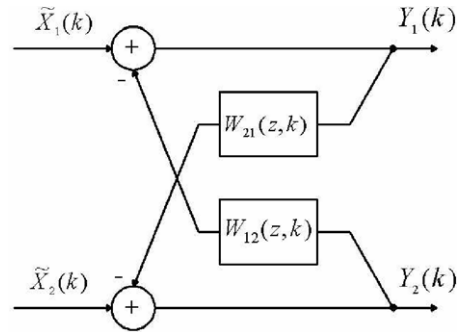


Fig. 11. Recurrent separation network.

the recurrent neural network architecture, Fig. 11 [15]. It is straightforward to derive relationships between the mixing filters and the separation filters in the Z domain:

$$\begin{aligned} W_{12}(z) &= G_{12}(z)G_{22}(z)^{-1}, \\ W_{21}(z) &= G_{21}(z)G_{11}(z)^{-1} \end{aligned} \tag{27}$$

or

$$\begin{aligned} W_{12}(z) &= G_{11}(z)G_{21}(z)^{-1}, \\ W_{21}(z) &= G_{22}(z)G_{12}(z)^{-1}. \end{aligned} \tag{28}$$

If the mixing filters $G_{11}(z)$, $G_{12}(z)$, $G_{21}(z)$ and $G_{22}(z)$ have zeros outside the unit circle, then non-causal realization of the separating filters $W_{12}(z)$ and $W_{21}(z)$ must be used in order to approximate unstable roots. Since any non-minimum phase system can be written as $G(z) = G_{\min}(z)G_{AP}(z)$, where $G_{\min}(z)$ is a minimum phase system and $G_{AP}(z)$ is an all-pass system [25], the problem of inverting the non-minimum phase system is to delay the inverting systems properly [26]. For the

recurrent separation network such delay is obtained by going to the frequency domain and performing the signal separation on the block by block basis. Therefore, we have applied here an adaptive frequency domain algorithm [24]. In order to identify the possible non-minimum phase problems we have applied the fourth-order cumulant based blind identification [21], of the mixing filters $G_{11}(z)$ and $G_{22}(z)$ that were modeled as the FIR filters of the 14th order. Provided that the input signals are non-Gaussian i.i.d. signals the coefficients of the FIR filter of the order L are obtained as [21]

$$h(i) = \frac{C_4y(L, 0, i)}{C_4y(L, 0, 0)}, \quad i = 0, \dots, L, \quad (29)$$

where $C_4y(L, 0, i)$ are the fourth-order cumulants of the output signal y . Since in our case the input signal is FM signal, that belongs to the sub-Gaussian class of signals, the fourth-order cumulants exist. Fig. 12 shows impulse response of such blindly identified FIR filter while the magnitude response is shown in Fig. 13 confirming the band-pass nature of the selective amplifier postfilters. Fig. 14 shows location of the zeros of such blindly identified FIR mixing filter. Obviously, there are zeros outside the unit circle. It should be noted that the zeros locations of the mixing filters $G_{11}(z)$ and $G_{22}(z)$ are influenced mainly by the character of the selective amplifiers impulse responses.

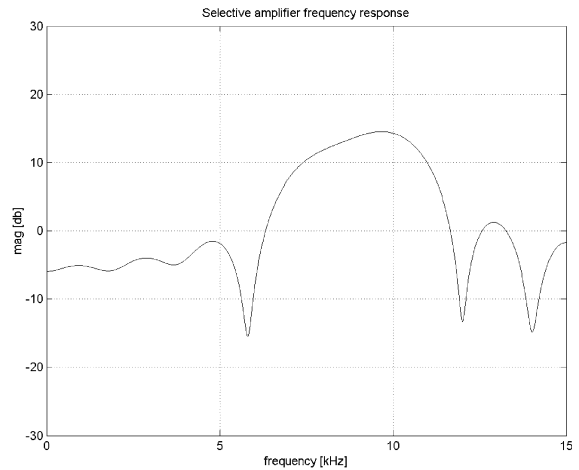


Fig. 13. Magnitude response of the blindly estimated FIR filter.

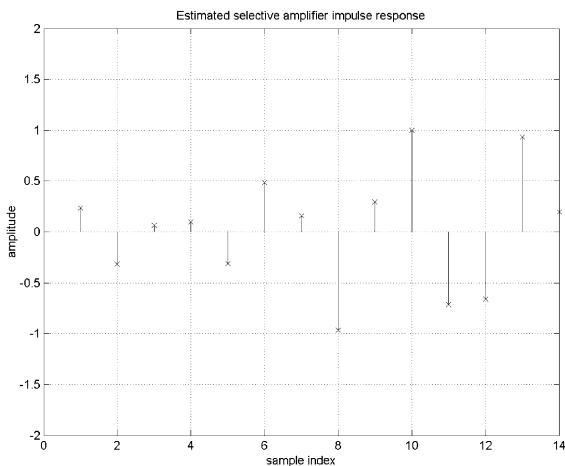


Fig. 12. Impulse response of the blindly estimated FIR filter.

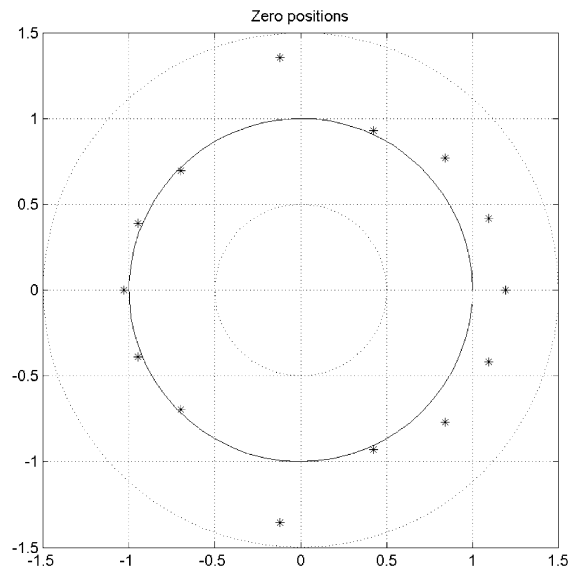


Fig. 14. Zeros of the blindly identified FIR filter.

One possible approach to blind source separation in multipath mixtures has been given in [32]. To recover the source signals we shall apply the slightly modified version of the adaptive frequency domain blind signal separation (BSS) algorithm developed by Back and Tsoi [23], that was itself the frequency domain extension of the time domain Herault–Jutten neural network [16,17]. The convolutive BSS problem is described with

$$x_i(k) = \sum_{j=1}^N \sum_{\tau=0}^L g_{ij}(\tau)s_j(k - \tau) \quad \forall 1 \leq i \leq M, \quad (30)$$

where M is the number of sensors, N is the number of sources and L is the windowed filter’s length. We shall assume here $M = N$ and g_{ij} s are the unknown FIR filters shown for the 2×2 case in Fig. 10. It is a general recommendation for any BSS method to apply it on the vector of the whitened or standardized data giving

$$\tilde{x} = Vx, \quad (31)$$

where $E[\tilde{x}\tilde{x}^T] = I$ and the whitening matrix V is obtained as

$$V = QA^{-1/2}Q^T, \quad (32)$$

where A and Q are eigenvalue and eigenvector matrices of the covariance matrix of the measured vector x , i.e.

$$E[xx^T] = QAQ^T.$$

The solution of the convolutive BSS problem is to find the matrix of filters that will transform in the

linear manner the standardized vector \tilde{x} into the output vector y with as much statistically independent components as possible. Transformation of the time domain convolutive model into the frequency domain results in the complex instantaneous model at each frequency band according to Fig. 15. In this way a linear convolutive problem (26)–(31) is transformed into the L complex instantaneous problems that can be solved with the BSS algorithms basically developed for the instantaneous mixtures [17,28–30]. Here L is the DFT length. There are, however, two problems associated with the convolutive mixtures that generally do not exist in the instantaneous case. The first one is scaling and permutation indeterminacy that is a feature inherent to the all BSS algorithms. The permutation indeterminacy becomes especially a serious problem if the convolutive problem is being solved in the frequency domain since the reconstruction of the time domain output signals requires all the frequency components of the same source. If the complete BSS algorithm is carried out in the frequency

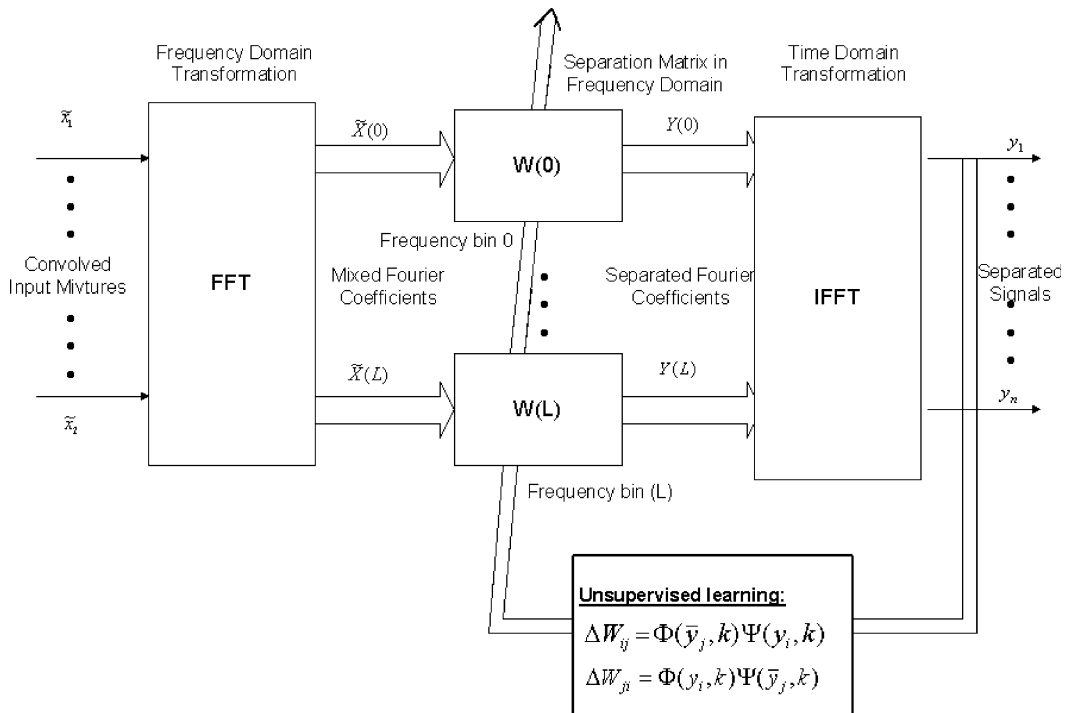


Fig. 15. Frequency domain adaptive blind source separation.

domain the very complicated solutions for the permutation indeterminacy are being proposed [31,33,34]. If however, filtering is done in frequency domain and separation criterion (independence, nonlinearities, HOS) is done in time domain the permutation and scaling problems do not exist. Examples of such methods are given in [23,24,26,34]. The second problem is the whitening effect that generally does not exist with the instantaneous mixtures. It can be avoided by the use of the recurrent neural network, Fig. 11, to perform the BSS task [15]. For the recurrent neural network, Fig. 11, the input–output equations at each frequency bin k are given with

$$Y(z, k) = \tilde{X}(z, k) - W(z, k)Y(z, k), \quad (33)$$

where Y and \tilde{X} are DFTs of y and \tilde{x} , W is the off-diagonal matrix, and k is the frequency bin index. When separation matrix $W(z, k)$ is updated according to some learning rules the vector of the recovered signals Y is based on (33), obtained as

$$Y(z, k) = (I + W(z, k))^{-1} \tilde{X}(z, k). \quad (34)$$

The frequency domain learning rules of the recurrent neural network developed by Back and Tsoi [23], are similar to the time domain Herault–Jutten neural network [17]

$$\Delta W_{ij} = \Phi(\bar{y}_j, k) \Psi(y_i, k), \quad (35)$$

where nonlinearities $\Phi(\circ)$ and $\Psi(\circ)$ are obtained as:

$$\begin{aligned} \Psi(y_i) &= \text{STFT}[\psi(y_i)], & \Phi(\bar{y}_j) &= \text{STFT}[\varphi(\bar{y}_j)], \\ y_i &= \text{ISTFT}(Y_i), & \bar{y}_j &= \text{ISTFT}(Y_j^*), \end{aligned} \quad (36)$$

where STFT means the Short-Time Fourier Transform that for the signal $x_i(k)$ is given with [36]

$$X_i^{\text{STFT}}(\omega, m) = \sum_{k=-\infty}^{\infty} x(k)w(k-m)e^{-jk\omega},$$

where $w(k)$ is the sliding window of the length L centered at $k = 0$ and m is the data block index. In the experiments reported in Section 5 we have used the Hanning window for $w(k)$. The STFT enables us to handle the non-stationary mixtures and signals. The convergence of the learning equation (35) is ensured provided that the source signals have even pdfs and the nonlinear functions $\Phi(\circ)$

and $\Psi(\circ)$ are odd. We have found, however, that modification of the learning rule (35) in the following manner improves the performance significantly [24]:

$$\begin{aligned} \Delta W_{ij} &= \Phi(\bar{y}_j, k) \Psi(y_i, k), \\ \Delta W_{ji} &= \Phi(y_i, k) \Psi(\bar{y}_j, k), \end{aligned} \quad (37)$$

where $i = 1, \dots, N-1$; $j = i+1, \dots, N$ and

$$\begin{aligned} \Phi(y_i) &= \text{STFT}[\varphi(y_i)], & \Phi(\bar{y}_i) &= \text{STFT}[\varphi(\bar{y}_i)], \\ \Psi(y_i) &= \text{STFT}[\psi(y_i)], & \Psi(\bar{y}_i) &= \text{STFT}[\psi(\bar{y}_i)], \\ y_i &= \text{ISTFT}(Y_i), & \bar{y}_i &= \text{ISTFT}(Y_i^*) \end{aligned} \quad (38)$$

and the nonlinearities $\varphi(\circ)$ and $\psi(\circ)$ are applied componentwise. In computing the STFT we will use the Cooley–Tuckey fast Fourier transform (FFT) algorithm. For the 2×2 case here proposed learning rule based on (37) is:

$$\begin{aligned} \Delta W_{12} &= \Phi(\bar{y}_2, k) \Psi(y_1, k), \\ \Delta W_{21} &= \Phi(y_1, k) \Psi(\bar{y}_2, k). \end{aligned} \quad (39)$$

It has been shown additionally for the instantaneous mixtures in [28,29] that the separation algorithms will still be efficient if $\psi(\circ)$ is linear function and $\varphi(\circ)$ is some odd nonlinear function. This significantly simplifies learning equation (39):

$$\begin{aligned} \Delta W_{21} &= \Phi(\bar{y}_2, k) Y_1(k), \\ \Delta W_{12} &= \Phi(y_1, k) Y_2^*(k), \end{aligned} \quad (40)$$

since one FFT and one IFFT less are required. It has been shown that from both the maximum likelihood principle [30] and the entropy maximization principle [35] the optimal choice of the nonlinearity $\varphi(\circ)$ is given with

$$\varphi(y_i) = -\frac{1}{p(y_i)} \frac{dp(y_i)}{dy_i}, \quad (41)$$

where $p(y)$ is the pdf of the data. This is in contradiction with the assumed blind scenario according to which we do not know the pdf of the data. But the learning equations will still be super-efficient [22], provided that the pdf of the data is an even function and the $\varphi(\circ)$ is an odd nonlinear function. For the super-Gaussian data the good choice is $\varphi(y) = \tanh(y)$ while for the sub-Gaussian data the good choice is $\varphi(y) = 2y + \text{sign}(y)y^2$.

5. Experimental results for the incoherent (heat) sources

Measured signals x_1 and x_2 are obtained on the basis of the two frequency modulated (FM) source signals s_1 and s_2 by means of the optical tracking device [3–7], whose schematic diagram is shown in Fig. 5 and photography of the working model is shown in Fig. 16. Deviation of the FM signal is proportional with the distance of the optical

source from the optical axis of the optical tracker. Spectrograms of the source signals s_1 and s_2 are shown in Figs. 17 and 18, respectively, while the spectrograms of the measured signals x_1 and x_2 are shown in Figs. 19 and 20, respectively. It can be seen from the spectrograms in Figs. 19 and 20 that two signals, corresponding with the associated single optical sources, exist simultaneously in the measured signals x_1 and x_2 . When an FM demodulator is applied on either signal x_1 or signal x_2 , only the IR optical source that was placed near the center of the field of view (FOV) can be dis-

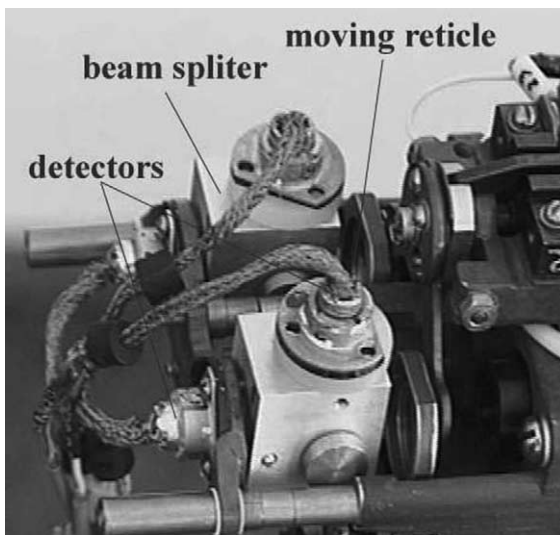


Fig. 16. Functional model of the modified reticle tracker.

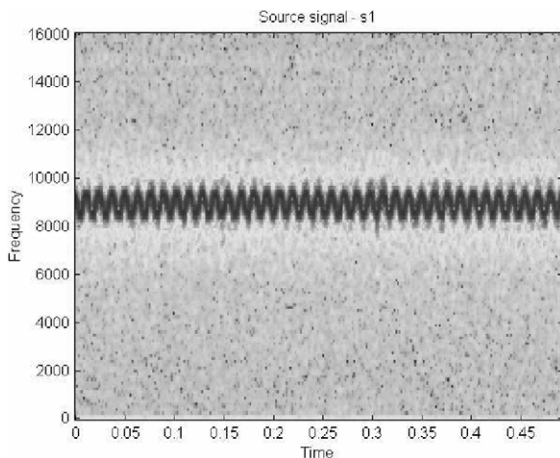


Fig. 17. Spectrogram of the signal s_1 .

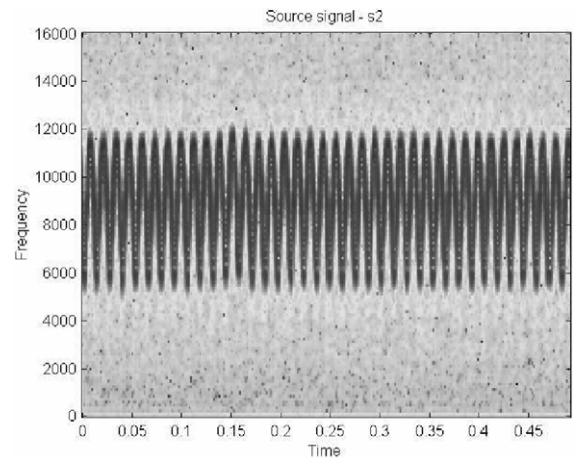


Fig. 18. Spectrogram of the signal s_2 .

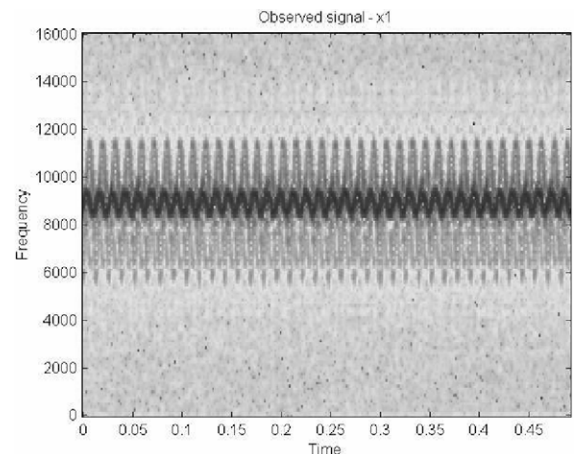


Fig. 19. Spectrogram of the signal x_1 .

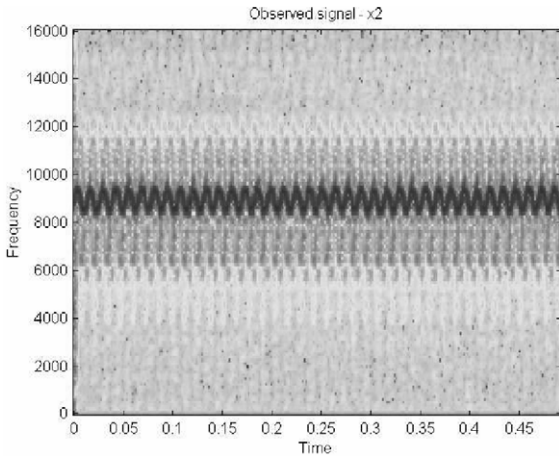


Fig. 20. Spectrogram of the signal x_2 .

criminated. If, however, the frequency domain based BSS algorithm, Eqs. (34)–(41), is applied on the signals x_1 and x_2 the influence of the IR source placed near the center of the FOV can be eliminated and both IR sources can be discriminated. Here, we have used the filter length of the 32 taps. In order to eliminate effects of the circular convolution the 32 zeros are added to the signal vectors prior to doing FFT. So the overall FFT length was $L = 64$. This FFT length introduces 1 ms delay in the tracking loop making it suitable for the real time tracking. We have done the frequency domain implementation using the overlap-save

technique with the overlap factor 0.5. The data were whitened before applying the BSS algorithm. Spectrograms of the output signals y_1 and y_2 , obtained according to Eq. (33) are shown in Figs. 21 and 22. It can be observed in the signal y_1 that the influence of the IR source placed near the center of the FOV is eliminated. Fig. 23 shows demodulated signals: the first one (with dick solid line) obtained after demodulation of the original source signal and the second one (with thin solid line) obtained after demodulation of the recovered signal with $\varphi(y) + 2y + \text{sign}(y)y^2$.

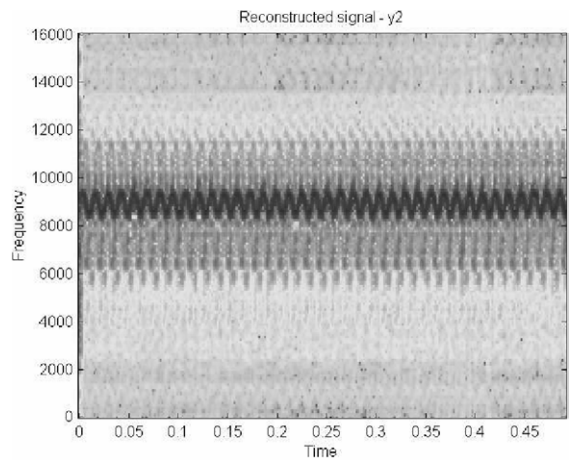


Fig. 22. Spectrogram of the signal y_2 .

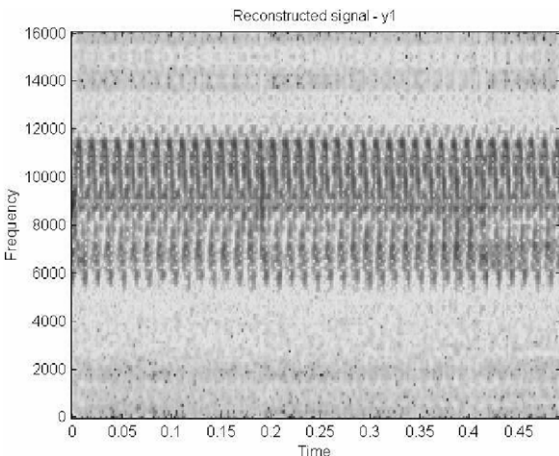


Fig. 21. Spectrogram of the signal y_1 .

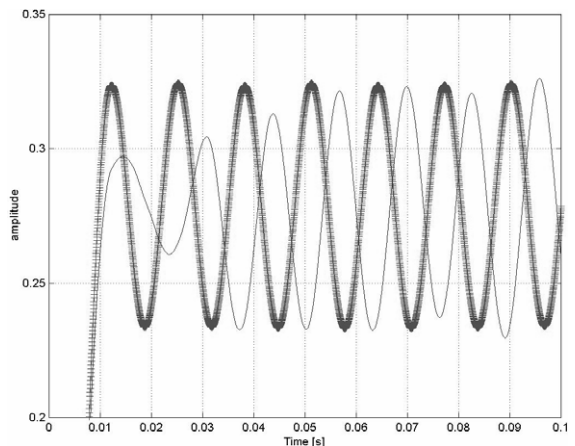


Fig. 23. Demodulated signals: dick line-original source; thin line-recovered source.

6. Conclusion

The beam splitter based modification of the reticle optical trackers is used for tracking and discrimination of the several optical sources. The mathematical framework called ICA is used for that purpose. The theoretical basis of the problem is formulated by using the statistical optics principles, the partial coherence theory and the Huygens–Fresnel principle. It has been shown analytically and verified experimentally that incoherent (heat) sources produce the linear ICA model which enables the application of the linear ICA theory to recover the unknown rfts that encode positions of the corresponding single optical sources. In a case of the partially coherent illumination by laser a nonlinear and highly nonstationary signal model is obtained. However, transformation into the linear model is possible in a special case when the partially coherent optical sources are not in a relative motion i.e. when the mutual degree of coherence is time invariant. If the coherence factor is time dependent we can introduce an additional source signal and apply the linear ICA algorithms developed for the undercomplete representation or an additional sensor must be used in order to have the same number of sensors and sources.

References

- [1] M. Born, E. Wolf, in: *Principles of Optics*, sixth ed., Cambridge University Press, Cambridge, UK, 1980, p. 491 (Chapter 10).
- [2] J.W. Goodman, in: *Statistical Optics*, Wiley, New York, 1985, p. 157 (Chapter 5).
- [3] I. Kopriva, A. Peršin, *Appl. Opt.* 38 (7) (1999) 1115.
- [4] H.H. Szu, I. Kopriva, A. Peršin, *Opt. Commun.* 176 (1–3) (2000) 77.
- [5] I. Kopriva, H.H. Szu, in: P. Pajunen, J. Karhunen (Eds.), *Proceedings of the 2nd International Workshop on Blind Signal Separation and Independent Component Analysis*, Helsinki, Finland, June 19–22, 2000, p. 51.
- [6] I. Kopriva, H.H. Szu, in: *Proceedings of the SPIE 4130, Infrared Technologies and Applications XXVI, SPIE's 45th Annual Meeting Optical Science and Technology*, San Diego, CA, USA, 30 July–4 August, 2000.
- [7] I. Kopriva, A. Peršin, in: *International Workshop on Blind Signal Separation and Independent Component Analysis*, Aussois, France, January 11–15, 1999, p. 31.
- [8] G. Olsson (Ed.), *Selected Papers on Reticles and Their Applications*, SPIE Milestone Series, vol. MS155, 1999.
- [9] R.D. Hudson Jr., in: *Infrared System Engineering*, Wiley, New York, 1969, p. 235 (Chapter 6).
- [10] H.K. Hong, S.H. Han, J.S. Choi, *Opt. Eng.* 36 (3) (1997) 883.
- [11] H.K. Hong, S.H. Han, J.S. Choi, *Opt. Eng.* 36 (8) (1997) 2341.
- [12] R.L. Driggers, C.E. Halford, G.D. Boreman, D. Lattman, K.F. Williams, *Appl. Opt.* 30 (7) (1991) 887.
- [13] R.L. Driggers, C.E. Halford, G.D. Boreman, *Appl. Opt.* 30 (19) (1991) 2675.
- [14] R.L. Driggers, C.E. Halford, G.D. Boreman, *Opt. Eng.* 30 (10) (1991) 1516.
- [15] K. Torkkola, in: *IEEE Workshop on Neural Networks for Signal Processing*, Kyoto, Japan, September 4–6, 1996, Institute of Electrical and Electronics Engineers, New York, 1996.
- [16] H.L. Nguyen Thi, C. Jutten, *Signal Process.* 45 (1995) 209.
- [17] C. Jutten, J. Herault, *Signal Process.* 24 (1991) 1.
- [18] H. Yang, S. Amari, A. Cihocki, *Signal Process.* 64 (1998) 291.
- [19] T.W. Lee, B.U. Koehler, in: *IEEE International Workshop on Neural Networks for Signal Processing*, FL, September 1997, Institute for Electrical and Electronic Engineers, New York, 1997.
- [20] A. Taleb, C. Jutten, S. Olympieff, in: *IEEE International Conference Acoustics, Speech, Signal Processing*, Seattle, Washington, May 1998, Institute for Electrical and Electronic Engineers, New York, 1998.
- [21] J.M. Mendel, *Proc. IEEE* 79 (1991) 278.
- [22] S. Amari, *IEEE Trans. Signal Process.* 47 (1999) 936.
- [23] A.D. Back, A.C. Tsoi, in: J. Vlontzos, J.N. Hwang, E. Wilson (Eds.), *Proceedings of the 1994 IEEE Workshop – Neural Networks for Signal Processing IV*, Institute of Electrical and Electronics Engineers, New York, 1994, p. 565.
- [24] I. Kopriva, Ž Devčić, H.H. Szu, in: *Proceedings of the INNS–IEEE Joint Conference on Neural Networks*, Washington, DC, July 15–19, vol. 1, 2001, p. 424 (ISBN:0-7803-7044-9).
- [25] S.J. Orfanidis, in: *Optimum Signal Processing*, second ed., MacMillan, New York, 1998, p. 143 (Chapter 3).
- [26] T.W. Lee, A.J. Bell, R. Orglmeister, in: *Proceedings of the International Conference on Neural Networks*, Houston, USA, 1997, p. 2129.
- [27] A. Jourjine, S. Rickard, Ö. Yilmaz, in: *Proceedings of the ICASSP*, Istanbul, Turkey, 2000, p. 2985.
- [28] S. Amari, J.F. Cardoso, *IEEE Trans. Signal Process.* 45 (11) (1997) 2692.
- [29] S. Amari, A. Cihocki, H.H. Yang, in: S. Haykin (Ed.), *Unsupervised Adaptive Filtering – Volume I Blind Source Separation*, Wiley, New York, 2000, p. 63 (Chapter 3).
- [30] D.T. Pham, *IEEE Trans. Signal Process.* 45 (1997) 1712.

- [31] C. Mejuto, A. Dapena, L. Castedo, in: P. Pajunen, J. Karhunen (Eds.), *Second International Workshop on Independent Component Analysis and Blind Signal Separation*, Helsinki, Finland, June 19–22, 2000, p. 315.
- [32] R.H. Lambert, C.L. Nikias, in: S. Haykin (Ed.), *Unsupervised Adaptive Filtering – Volume I Blind Source Separation*, Wiley, New York, 2000, p. 377 (Chapter 9).
- [33] H.C. Wu, J.C. Principe, in: J.F. Cardoso, Ch. Jutten, Ph. Loubaton (Eds.), *First International Workshop on Independent Component Analysis and Signal Separation*, Aussois, France, January 11–15, 1999, p. 245.
- [34] V. Capdevielle, C. Serviere, J.-L. Lacoume, in: *Proceedings of the ICASSP95*, 1995, p. 2080.
- [35] A.J. Bell, T.J. Sejnowski, *Neural Comput.* 7 (1995) 1129.
- [36] G. Zelniker, F.J. Taylor, in: *Advanced Digital Signal Processing – Theory and Applications*, Marcel Dekker Inc., New York, 1994, p. 384.